High-resolution x-ray scattering study of platinum thin films on sapphire

1998 J. Phys.: Condens. Matter 10 717

(http://iopscience.iop.org/0953-8984/10/4/002)

J. Phys.: Condens. Matter **10** (1998) 717–730. Printed in the UK PII: S0953-8984(98)83046-4

High-resolution x-ray scattering study of platinum thin films on sapphire

A Nefedov†, A Abromeit, Ch Morawe and A Stierle

Institut für Experimentalphysik/Festkörperphysik, Ruhr-Universität Bochum, D-44780 Bochum, Germany

Received 3 April 1997, in final form 3 October 1997

Abstract. Platinum films in the thickness range 20–500 Å have been sputtered onto $(11\bar{2}0)$ sapphire substrates at different substrate temperatures T_S. The structural properties of these films have been studied by high-resolution x-ray scattering techniques. Information about the total thickness of the film and about the surface and interface roughnesses has been determined by means of x-ray specular reflectivity measurements. The films sputtered at $T_S \geqslant 300$ °C have shown Laue oscillations about the Pt(111) Bragg peak. The average thickness of coherently stacked lattice planes L_C has been compared with the total film thickness t_{tot}, obtained from the reflectivity measurements. The epitaxial relationship between the platinum film and the sapphire substrate has been determined using in-plane x-ray diffraction. It was demonstrated that Pt epitaxial films include two in-plane orientations related by a 180° rotation. Both anisotropic compression in the $[1\bar{1}0]$ direction and anisotropic expansion in the [111] direction were observed for these films. A correlated variation of some structural parameters with the substrate temperature T_S was found.

1. Introduction

Thin metal films are of considerable interest in different fields of science and technology and several applications of platinum films have been recently demonstrated. Firstly, they can be used as a model system for the analysis of catalytic reactions on solid-state surfaces and this fact has been demonstrated for a variety of substrates, including $TiO_2(110)$ [1], ZnO(0001) [2], amorphous Al_2O_3 and α-$Al_2O_3(0001)$ [3]. Another possible application of thin Pt films is their use as a seed layer for growth of fcc metal films on insulating substrates. In the paper [4], the growth and characterization of Pt(111) on basal-plane sapphire has been described. It has been shown that this epitaxial metal–insulator combination, with suitable growth conditions, provides a near-ideal seed film for the epitaxial growth of a wide variety of structures for giant magnetoresistance study. It also provides the basis for a variety of other epitaxial magnetic structures including multilayers and alloys which exhibit perpendicular magnetic anisotropy.

Pt films have been obtained by a variety of techniques, including plasma-arc deposition [5], electron-beam deposition [6], magnetron sputtering [7, 8] and chemical vapour deposition [9]. In the paper [10], Pt films were grown on $Al_2O_3(0001)$ using ion-beam sputtering and the temperature dependence of the growth as well as its effect on the resulting morphology have been studied. It has been shown that the substrate temperature T_S is a

† Permanent address: RRC 'Kurchatov Institute', 123182 Moscow, Russia.

0953-8984/98/040717+14$19.50

fairly sensitive parameter and that deviations from its nominal value of 600 °C result in very different growth characteristics.

In the paper [9], Pt films were grown on (0001), $(11\bar{2}0)$ and $(01\bar{1}2)$ sapphire single-crystal substrates by chemical vapour deposition at temperatures T_S between 400 and 800 °C. The epitaxial growth was achieved at deposition temperatures between 500 and 600 °C with the addition of oxygen to the source vapour. The film orientation and epitaxial relationships between the films and substrates were determined by means of x-ray diffraction, x-ray pole figures and reflection high-energy electron diffraction. However, the work in [9] was restricted to high temperatures $T_S \geqslant 400$ °C and thick films (>1000 Å) and no studies were made of the early stages of the epitaxy. In order to elucidate the influence of T_S on the growth morphology of Pt, we investigated in detail the structure of sputtered films for wide ranges of the substrate temperatures and film thicknesses.

2. Experimental techniques

Single-crystalline $(11\bar{2}0)$ sapphire with a miscut angle below 1° and a mosaicity around 0.004° was used as the substrate. Before deposition all of the substrates were cleaned ultrasonically in acetone and ethanol. Then, they were annealed up to 500 °C under a high vacuum and plasma etched directly before sputtering. Platinum films were deposited by rf sputtering (13.56 MHz) in a high-vacuum environment with a base pressure of 3×10^{-8}–1×10^{-7} mbar after LN_2 cooling, at different substrate temperatures T_S equal to 30 °C, 100 °C, 300 °C and 600 °C. T_S was controlled by a PID controller supplying a resistive heater on top of the substrate holder. The 99.99% pure Pt target was mounted 8 cm below the substrates. Sputtering was carried out in an atmosphere of 99.999% pure Ar at a pressure of 5×10^{-3} mbar. The electrical power of the discharge was 100 W which led to a sufficiently low sputtering rate of 0.15 Å s^{-1}. The nominal thicknesses of the Pt films were 20 Å, 100 Å and 500 Å. The estimation of this thickness was carried out by measuring the deposition time. All of the samples were removed from the growth chamber at room temperature. The sputtering set-up was described in detail in [11].

X-ray scattering is most suitable for detailed structural characterization of thin films, since it is a non-destructive method providing surface as well as bulk information on one and the same sample. Two kinds of scan are carried out: low-angle and the wide-angle scans. Information about the film thickness, the interfacial roughnesses and the electron density profile perpendicular to the film plane irrespective of the crystallinity of the film is obtained via radial scans (Θ–2Θ scans) in the small-angle regime (reflectivity measurements). The wide-angle radial scans at a reciprocal-lattice point (Bragg scans) normal to the growth direction provide information about the nature of the films (polycrystalline or single crystalline) and in the latter case also about the predominant texture. The transverse scans through the Bragg peak provide information on the out-of-plane mosaicity of the film.

We used a double-axis diffractometer based on an 18 kW rotating-anode generator (Cu Kα radiation, $\lambda = 1.54$ Å) with a graphite monochromator in the incident beam. The monochromator reduced only the background and Kβ radiation, and not the contribution of the Kα_2 line. A NaI(Tl) scintillation counter was used to detect the radiation. In the wide-angle region the Bragg angle of the monochromator is near the Bragg angles of the film and the substrate. This leads to a nearly dispersion-free situation and the resolution is limited only by slits. The resolution of the diffractometer was $\Delta\, 2\Theta = 0.03°$ at $2\Theta = 37.8°$ as obtained from the resolved Kα_1 linewidth of the sapphire $(11\bar{2}0)$ reflection. In the reflectivity measurements the resolution is limited by geometrical factors, such as the slit sizes and the monochromator–detector distance. As a good compromise between poorer

resolution and loss of intensity we have chosen an angular beam divergence of 0.02°.

Since the information about the in-plane structure of these films is very important for understanding the Pt film growth process, the in-plane Bragg scans have been carried out for glancing angles of incidence in order to determine the epitaxial relationship of the platinum film to the substrate, average crystallite sizes and mosaic distributions of the crystallites with respect to the preferential orientation. In our experiments the angle of incidence α_i was kept constant and equal to the critical angle for the total external reflection from platinum. Using a soller slit of 0.15° horizontal divergence, the radial and transverse resolutions were about 0.23° and 0.10°, respectively.

3. Experimental results

3.1. X-ray reflectivity studies

The intensity of specularly reflected x-rays at small angles provides information on the average electron density profile of the material studied in the direction along the surface normal. Assuming a certain electron density profile, the reflectivity can be calculated as a function of the scattering vector. In this work we calculated the x-ray reflectivity by means of a dynamic treatment, generally referred to as the Parratt formalism for x-ray reflectivity [12], using optical boundary conditions for reflection, refraction and transmission at each interface. The Parratt formulae were modified according to Névot and Croce [13] to take the roughness σ into account; it is defined as the root mean square of the electron density height fluctuation at the interface. Before fitting, the diffuse non-specular intensity was subtracted from the data.

Table 1. The thickness and roughness parameters as well as the values of the electron density, reduced to that of bulk platinum, obtained from the fits of the x-ray reflectivity data.

Nominal thickness (Å)	T_S (°C)	σ_{surf} (Å)	ρ/ρ_{Pt}	t_{surf} (Å)	σ_{int} (Å)	ρ/ρ_{Pt}	t_{int} (Å)	σ_{Pt} (Å)	ρ/ρ_{Pt}	t_{Pt} (Å)	σ_{sub} (Å)
20	30	2	—	—	—	—	—	—	1	21	3
20	300	2	—	—	—	—	—	—	1	25	1
20	600	5	—	—	—	—	—	—	0.42	27	3
100	30	2	0.85	10^{-14}	—	—	—	21	1	106	3
100	300	2	0.5	10^{-11}	—	—	—	9	1	114	5
100	600	11	0.88	105	—	—	—	10^{-7}	1	14	2
500	30	5	0.23	12	—	—	—	4	1	530	9
500	300	10	0.27	16	—	—	—	13	1	509	3
500	600	10^{-7}	0.3	25	6	0.45	21	49	1	533	16

The reflectivity data for the films with nominal thickness equal to 20 Å, sputtered at different substrate temperatures T_S, are shown in figure 1(a) with a logarithmic intensity scale. The open circles represent the data points and the solid lines are fits. The inset shows the electron density profiles normal to the physical surface resulting from the fit. From the inset we can see that the 20 Å films sputtered at $T_S = 30$ °C and 300 °C (solid lines) have values of the electron density close to the bulk platinum value and a good layer smoothness with small values of the surface and interface roughnesses. All of the parameters obtained from the fit are presented in the table 1. For the sample grown at 600 °C (the dashed line) the situation is drastically different. The best fit yields a value of the electron density that

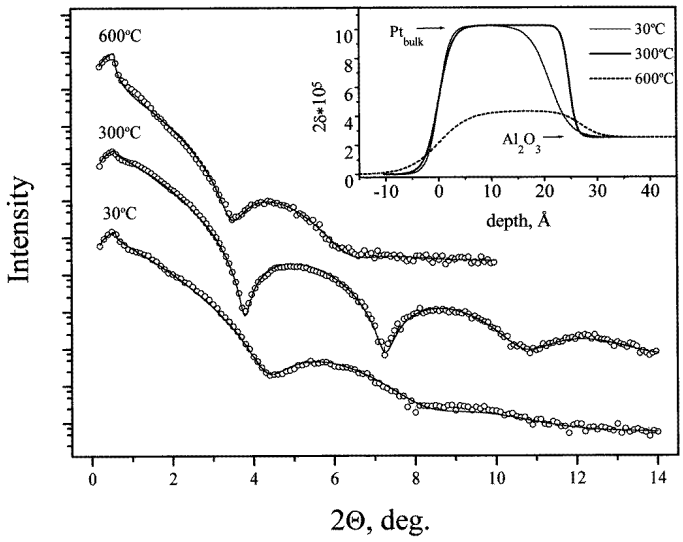

(a)

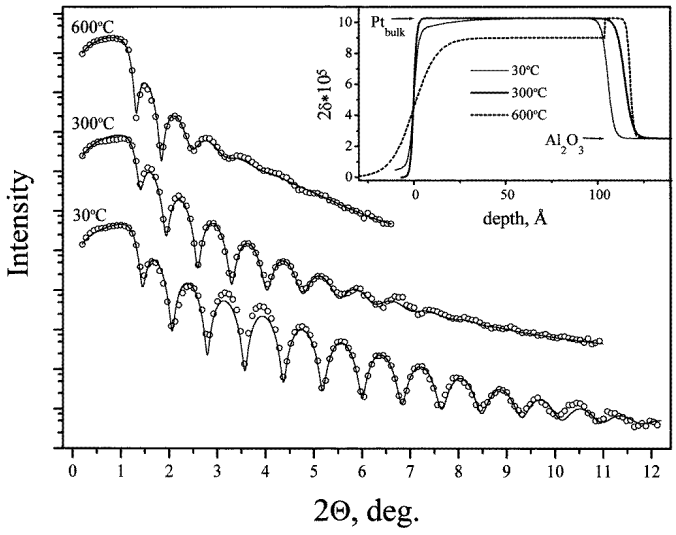

(b)

Figure 1. The x-ray reflectivities of Pt films 20 Å (a), 100 Å (b) and 500 Å (c) thick on sapphire, sputtered at different substrate temperatures. The solid lines show fits of calculated density profiles to the data points obtained using the dynamic formalism. The electron density profiles used for the fits are given in the insets.

is only 42% of that for the bulk platinum. We assume that the film is not homogeneous but consists of islands of platinum.

The reflectivity data for the films 100 Å and 500 Å thick (figures 1(b), 1(c)) exhibit a clear edge of total external reflection at $2\Theta = 1.15^{\circ}$. For the Pt films 100 Å thick (figure 1(b)) sputtered at the substrate temperatures $T_S = 30\ ^{\circ}\mathrm{C}$ and 300 °C the electron density profile (the solid lines in the inset) consists of a thick layer with the bulk Pt electron

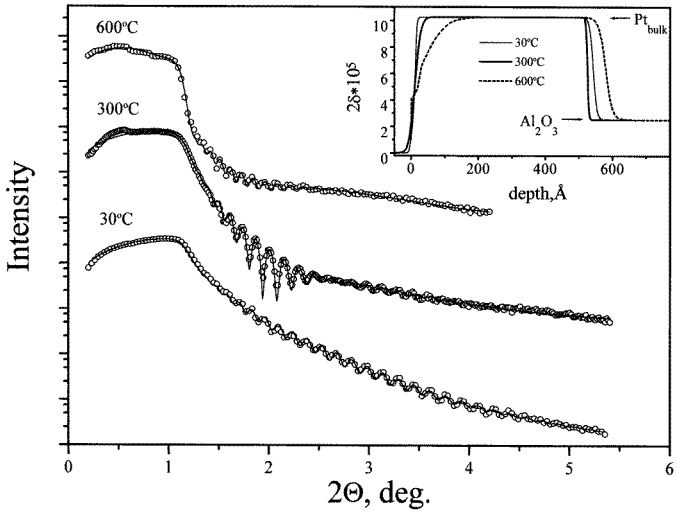

(c)

Figure 1. (Continued)

density covered by a surface layer of thickness t_{surf} with a reduced electron density. For these films the parameter t_{surf} reaches low, unphysical values (see table 1) and the value of the interface roughness σ_{int} is too large to allow the assumption of a Gaussian height fluctuations at the interface. Therefore what is needed for this layer is just a better description of the surface roughness, and here the surface layer (t_{surf}), surface (σ_{surf}) and interface (σ_{int}) roughnesses represent the surface roughness of the platinum film. The profile corresponding to the film sputtered at $T_S = 600$ °C (the dashed line) differs from the previous case. The main part of the platinum film (105 Å) has an electron density value equal to 88% of the bulk platinum electron density.

Figure 1(c) shows the reflectivity data for samples 500 Å thick. The amplitude modulation of the reflectivity is clearly seen from the damping of the oscillations at $2\Theta = 2.65^\circ$ for the sample sputtered at $T_S = 300$ °C. This modulation is caused by the presence of a surface layer and, therefore, it is necessary to introduce an additional layer into the model. For the 500 Å film, sputtered at the substrate temperature $T_S = 600$ °C, a second layer with an intermediate electron density should be introduced between the surface and the bulk layer. The need for the second layer in the surface region indicates that the condition $q_z\sigma \ll 1$, which is used in the Névot–Croce formalism, is invalid for this film, where $q_z = (4\pi/\lambda)\sin\Theta$ is the normal component of the scattering vector. The introduction of the intermediate layer is therefore only the first step towards a more refined electron density profile which may be obtained by dividing the surface region into a large number of thin sheets with different values of the electron density.

3.2. Out-of-plane Bragg measurements

For thin films with a finite number N of coherently scattering lattice planes the Bragg reflection shows typical fringes of Laue oscillations given [14] by

$$\mathcal{L}_N = \sin^2(q_z N d/2)/\sin^2(q_z d/2)$$

where d is the spacing and q_z is the normal component of the scattering vector.

In general, the film does not consist of a constant number of perfectly stacked lattice planes of infinite extent. Instead, the lateral extent is finite and the number of coherently scattering planes varies from stack to stack. In order to arrive at a more realistic model we should take into account fluctuations in the number N of coherently scattering lattice planes. In our model we assumed a Gaussian distribution of N, and an incoherent superposition of the Laue functions $\mathcal{L}_N$ is carried out, leading to the following result [15]:

$$I \sim \sum_N \mathcal{L}_N(\pi\ \Delta N)^{-1/2} \exp[-(4\ln 2)(N - N_0)^2/(\Delta N)^2] \tag{1}$$

where N_0 is the average number of coherently scattering lattice planes and ΔN is the standard deviation of the Gaussian distribution.

Using expression (1) for fitting the experimental data points, only three parameters are required: the average number N_0 of coherently scattering lattice planes, the interplanar distance d and the mean square fluctuation ΔN about N_0. These parameters can be obtained with some reliability because each one has a distinctive influence on the diffraction pattern: d corresponds to the angular position of the Bragg reflection and N_0 and ΔN determine the period and damping of the oscillations, respectively. Multiplying the values of N_0 by d we obtain the average thickness of coherently stacked lattice planes $L_C = N_0 d$ in the Pt film. Here the parameter $\sigma_{coh} = \sqrt{8\ln 2}\,\Delta N\, d$ is a measure of the lattice 'roughness' of the coherently scattering planes.

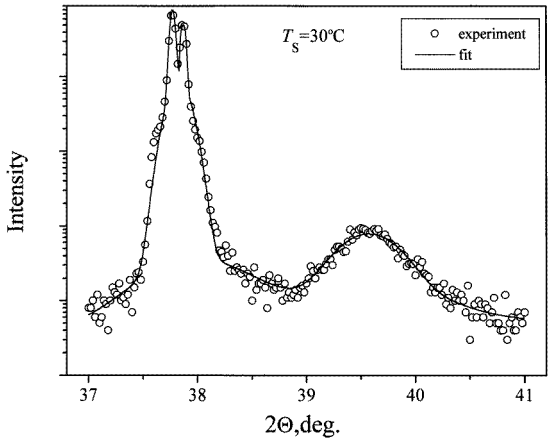

Figure 2. The Bragg scans of the Pt(111) peak for the sample sputtered at the substrate temperature $T_S = 30\ ^\circ$C with the total thickness equal to about 500 Å. The open circles are the experimental data and the solid line represents a fit according to expression (1). The sharp reflection corresponds to the diffraction from the sapphire substrate.

Figure 2 shows a profile of Pt(111)/$Al_2O_3(11\bar{2}0)$ peaks for the 500 Å film grown at $T_S = 30\ ^\circ$C. The open circles are the experimental data and the solid line represents a fit. The sharp reflection corresponds to the diffraction from the sapphire substrate. We can see a broad Bragg peak of the Pt(111) reflection at $2\Theta = 39.5^\circ$ without any Laue oscillations. It is typical for polycrystalline samples and its position gives the value of the spacing $d = 2.276$ Å.

When the grain size becomes smaller than the film thickness, there is more than one grain connecting the two film boundaries. Then the parameter $N_0 d$ corresponds to the average grain size rather than to the average thickness of coherently scattering lattice planes, and

the parameter σ_{coh} is a measure of the variation of the grain sizes. We have found from the fit that the platinum film consists of grains with sizes from 30 Å to 140 Å. Curves with a similar shape were obtained for other films deposited at this substrate temperature, but the fitting of these curves is impossible, since the intensities of the Pt(111) Bragg peaks are weaker, although these peaks are still visible.

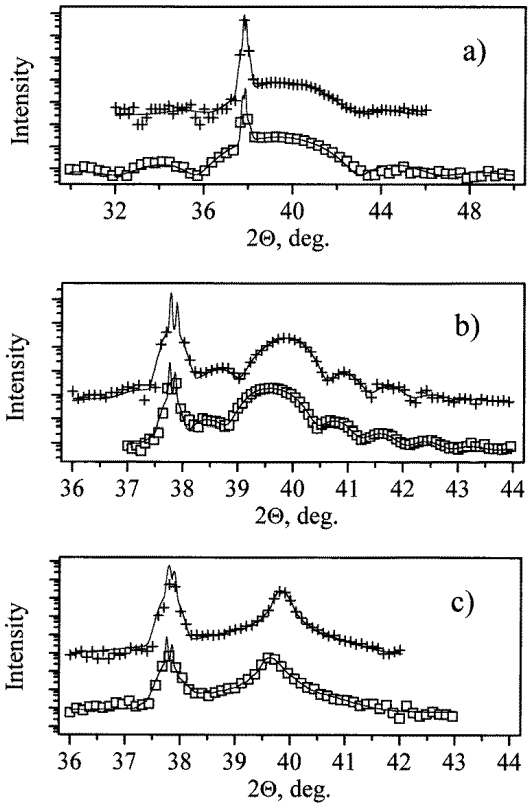

Figure 3. Radial scans of the Pt(111) Bragg peak for samples sputtered at the substrate temperatures $T_S = 300$ °C (squares) and $T_S = 600$ °C (crosses). The solid lines represent the fit. The total thicknesses are about 20 Å (a), 100 Å (b) and 500 Å (c). The sharp reflection corresponds to the diffraction from the sapphire substrate.

Figure 3 shows Bragg scans from Pt films with the nominal thicknesses 20 Å (a), 100 Å (b) and 500 Å (c), grown at the substrate temperatures $T_S = 300$ °C (squares) and $T_S = 600$ °C (crosses). The Pt(111) Bragg peak is flanked by several Laue oscillations. The sharp reflection on the left-hand side corresponds to the diffraction from the sapphire substrate. In figure 3(c), which shows the Pt(111) Bragg profile of the 500 Å film, the oscillations are still visible; however, their damping indicates the presence of a high density of defects (clusters, twin boundaries etc). Up to three additional Gaussian profiles of intensity, which correspond to the diffuse scattering at these defects, should be assumed for the increased intensity below the Bragg peak in order to improve the fit. The parameters d, N_0 and ΔN deduced from the fit as well as L_C and σ_{coh} are collected together in table 2.

As mentioned above, the Bragg intensities point to a significant texture, depending on the growth temperature. The texture was determined directly by scanning the Pt(111) peak

Table 2. The spacing d, the average number N_0 of coherently scattering lattice planes and the parameter ΔN describing the Gaussian fluctuations of N_0, as well as the coherence length L_C and σ_{coh}, which are used for obtaining the best fit of the Pt(111) Bragg peaks of the films.

Nominal thickness (Å)	T_S (°C)	d (Å)	N_0	ΔN	L_C (Å)	σ_{coh} (Å)
500	30	2.276	37	23.5	84.2	53.5
100	100	2.276	27	20.4	61.5	46.5
20	300	2.290	10.7	1	24.5	5.4
100	300	2.273	51	3	115.9	16.0
500	300	2.274	214	4	487	21.2
20	600	2.277	12	2.5	27.3	13.4
100	600	2.263	51.8	4.25	117.2	22.8
500	600	2.264	256	8	580	42.4

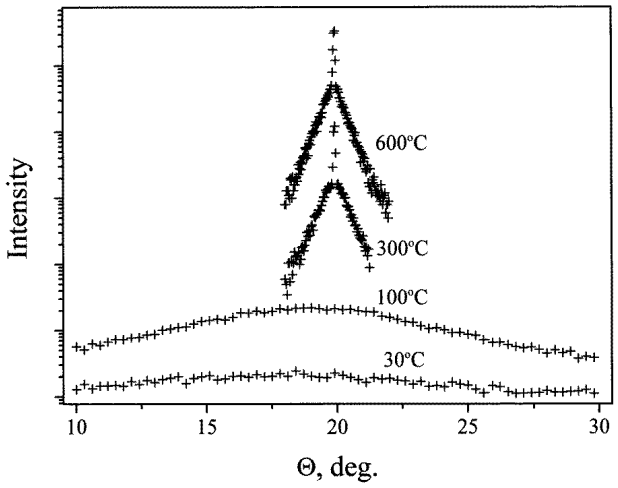

Figure 4. Rocking curves for 100 Å Pt films grown at different substrate temperatures T_S, with a logarithmic intensity scale.

in the transverse direction, i.e. by performing the rocking scan with a fixed detector at a 2Θ-position and stepping the Θ-position of the sample. The rocking curves for the platinum films that were 100 Å thick, grown at different substrate temperatures T_S, are shown in figure 4, with a logarithmic intensity scale.

Analysing the out-of-plane texture by taking rocking curves, we have found again differences between films deposited at low (30–100 °C) and high (300–600 °C) temperatures. In the first case we have smooth Gaussian-shaped rocking curves with the full width at half-maximum (FWHM) equal to about 10° ($T_S = 30$ °C) and 3° ($T_S = 100$ °C). High-temperature samples, in contrast, exhibit rocking curves consisting of two contributions: a very sharp component with a FWHM of 0.07° superimposed on a broad component with a FWHM of 0.7°. The broad component may arise from a distribution of structural defects such as twin boundaries and local deformation of the lattice planes. This is a characteristic for all of the samples but with different ratios of the integrated intensities for the sharp and broad components. With increasing film thickness the integrated intensity of the sharp component decreases in comparison with that of the broad component.

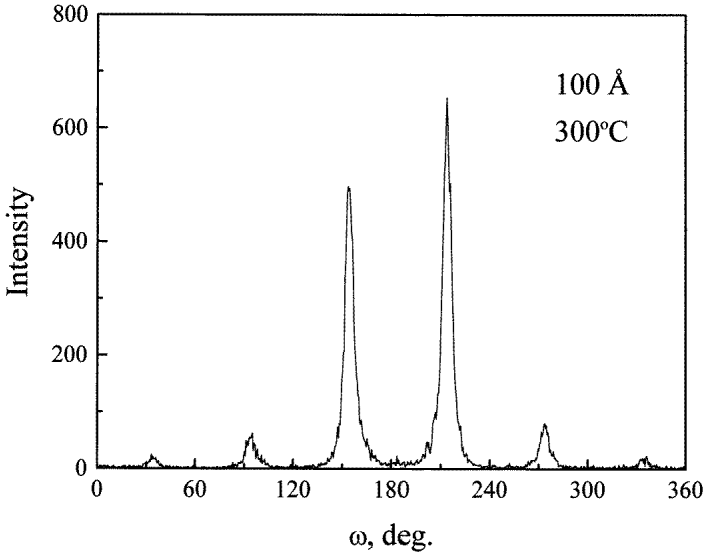

Figure 5. The rotational or ω-scan of the Pt($2\bar{2}0$) in-plane reflection of a 100 Å film deposited at $T_S = 300$ °C. The reflections are separated by 60°, indicating a sixfold symmetry.

3.3. Surface x-ray diffraction

It should be noted that the out-of-plane rocking scans, described above, only probe the texture and the mosaicity normal to the film plane. Therefore, nothing can be concluded from these scans about the in-plane structure. In analogy to the previous paragraph, we have measured the in-plane coherence length and the crystal orientation in the surface scattering configuration.

Figure 5 shows an ω-scan where the sample is rotated about an axis parallel to the film normal and the detector is kept fixed at the Pt($2\bar{2}0$) Bragg position for a film 100 Å thick deposited at $T_S = 300$ °C. The Pt reflections appear at 36°, 96°, 156°, 216°, 276° and 336°, in accordance with the sixfold symmetry, indicating rotational twinning with some grains rotated by 180° round the [111] axis with respect to the others. The varying intensity is caused by a slight misalignment of the sample.

A scan like that shown in figure 5 was also carried out for the Pt($22\bar{4}$) Bragg position, which allows one to perform a mapping of the in-plane reciprocal lattices of platinum and sapphire and, in particular, to determine the epitaxial relationships between the Pt film and the substrate. The result is shown in figure 6, where the sapphire in-plane Bragg peaks are indicated as small dots and the Pt peaks are streaks proportional to the in-plane mosaicity of the films. According to this figure, the Pt[$11\bar{2}$] and Pt[$\bar{1}\bar{1}2$] axes are aligned parallel to the Al_2O_3 [0001] axis, and the Pt[$1\bar{1}0$] axis is parallel to the Al_2O_3 [$1\bar{1}00$] axis. This suggests R180° twinning about the [111] axis, as observed in prior work for Pt(111)/Al_2O_3(0001) [4] and for Pt/sapphire($11\bar{2}0$) samples studied in [9]. The origin of the rotational twinning could be steps on the sapphire substrate. Figure 7 demonstrates the radial scan through the Pt($2\bar{2}0$) Bragg peak for the 100 Å film of platinum, grown at 300 °C. From the position of this peak we have obtained the interplanar distance $d^*_{2\bar{2}0} = 1.374$ Å, which is very close to the spacing $d_{1\bar{1}00}$ of sapphire, and from the radial width we have estimated the in-plane coherence length to be about 70 Å.

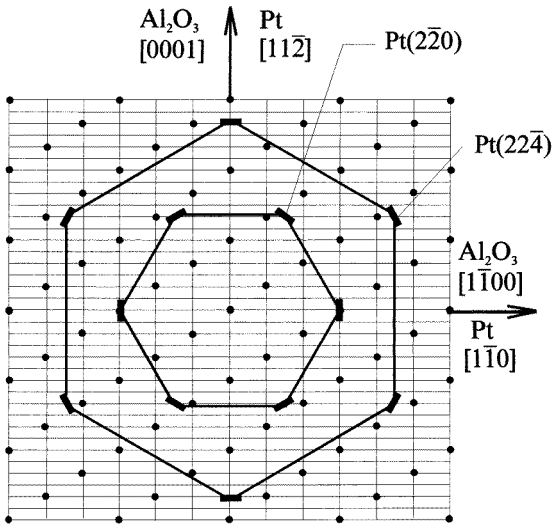

Figure 6. Epitaxial relationships between the platinum film and the (11$\bar{2}$0) sapphire substrate. The background grid and small dots indicate the reciprocal lattice of the sapphire substrate. Bold lines and streaks mark the Pt reciprocal space. Each of the six Pt(2$\bar{2}$0) and (22$\bar{4}$) reflections lie on a hexagon. The hexagons are rotated by 30° with respect to each other.

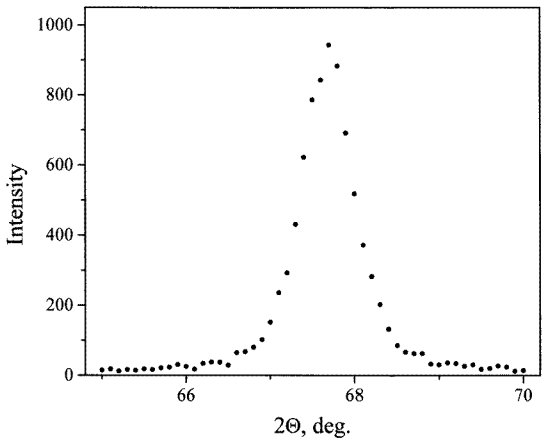

Figure 7. A radial scan of the Pt(2$\bar{2}$0) Bragg peak for a film 100 Å thick sputtered at the substrate temperature $T_S = 300$ °C.

4. Discussion

The average thickness of coherently stacked lattice planes L_C versus the total film thickness t_{tot}, obtained from the reflectivity measurements, is shown in figure 8. For films deposited at high substrate temperatures ($T_S = 300$ °C (open circles) and $T_S = 600$ °C (triangles)) the coherence length L_C equals the total film thickness t_{tot} (the dashed line in this figure corresponds to the equation $L_C = t_{tot}$). For the films 500 Å thick (for both temperatures) it is difficult to obtain precise values for L_C as well as t_{tot} for reasons mentioned in the previous section, but within experimental error this equality is valid too. This means that

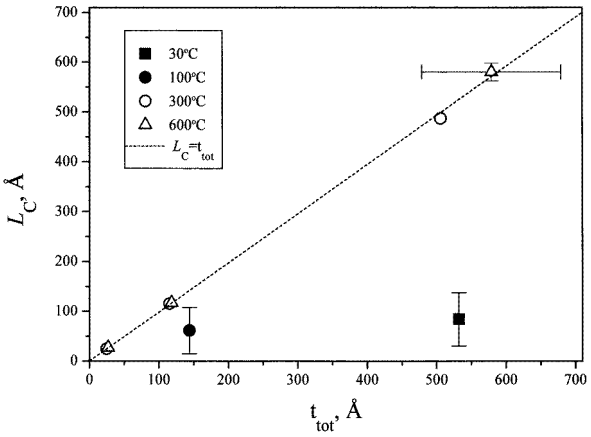

Figure 8. The coherence length of the Pt film thickness obtained from the Laue oscillations versus of the total film thickness obtained from the reflectivity measurements. The dashed line corresponds to the equation $L_C = t_{tot}$.

at these substrate temperatures the films mainly consist of grains that were grown from the substrate up to the surface. As we mentioned earlier, for the films sputtered at low substrate temperatures ($T_S = 30$ °C and $T_S = 100$ °C) the parameter $N_0 d$ represents only the average grain size, which turns out to be independent of the film thickness (filled squares and filled circles, respectively). Here the error bars show the range of grain sizes.

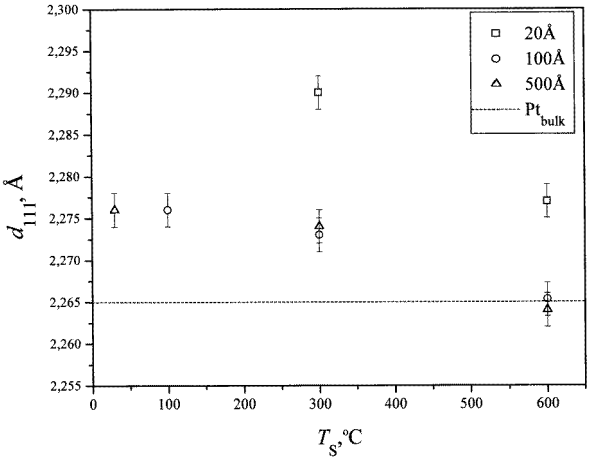

Figure 9. The spacing of platinum in the growth direction d_{111} as a function of the substrate temperature T_S. The dashed line indicates the bulk value.

The interplanar distance in the growth direction d_{111} versus T_S is plotted in figure 9. The dashed line indicates the spacing of the Pt(111) bulk value (2.265 Å). For the films with thicknesses 100 Å (circles) and 500 Å (triangles), deposited at 600 °C, d is nearly equal to the bulk value, but for lower T_S, an increase of the spacing up to the value $d = 2.275 \pm 0.002$ Å takes place, corresponding to expansion in the growth direction. For the films 20 Å thick the situation is a little different. For $T_S = 600$ °C, the film spacing

equals the value $d = 2.277$ Å (which is close to the values for thicker films, deposited at low T_S), but for $T_S = 300$ °C an additional increase of the film spacing up to $d = 2.290$ Å takes place.

In order to understand the reasons for this expansion of Pt films, we compared the lattice parameters of sapphire and Pt in directions parallel to the film surface. For the sapphire the spacing in the [0001] direction, d_{0006}, equals 2.1648 Å. In the Pt(111) plane the atomic row distance in the $[11\bar{2}]$ direction is $3d_{22\bar{4}} = 2.4024$ Å, which leads to a misfit of 11%. In the $[1\bar{1}00]$ direction the relevant distance is $d_{3\bar{3}00} = 1.373\,76$ Å, which matches very well with the bulk Pt value $d_{2\bar{2}0} = 1.387$ Å (the misfit is about 1%). Moreover, as we stated above, from the in-plane scan we have obtained for thin films $d^*_{2\bar{2}0} = 1.374$ Å. In the case of the epitaxy, the Pt film is compressed in the $[1\bar{1}0]$ direction by the amount $\Delta d_{2\bar{2}0} = d_{2\bar{2}0} - d_{3\bar{3}00}$ and, hence, the expansion of the interplanar distance in the growth direction is a result of strain in the film plane, according to Poisson's ratio. These intrinsic strains have also been observed in other metallic films [16, 17]. Since $\Delta d_{111}/d_{111} = \mu\,\Delta d_{2\bar{2}0}/d_{2\bar{2}0}$, where $\mu = 0.36$ is Poisson's ratio for Pt, we obtain the spacing in the growth direction $d^*_{111} = d_{111}(1 + \mu\,\Delta d_{2\bar{2}0}/d_{2\bar{2}0}) = 2.273$ Å. Within the experimental error, this spacing is equal to the values which we have obtained from the fit of the experimental curves for the films with the nominal thicknesses 100 Å and 500 Å sputtered at $T_S \leqslant 300$ °C.

For films grown at $T_S = 600$ °C island growth is preferred, which leads to the formation of a lot of grain boundaries. Therefore the growth of the film at this temperature takes place with bulk parameters of spacings in accordance with the mechanism of a stress relaxation via the grain boundaries [18]. The strong diffuse scattering in the rocking curves for these films confirms the presence of these boundaries. It is in accordance with the results obtained in [4], where Pt nucleates as islands at 600 °C.

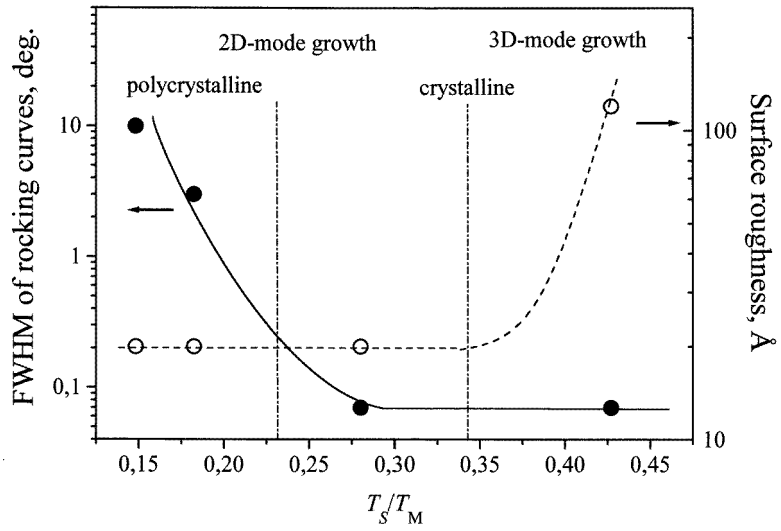

Figure 10. The dependencies of the surface roughness σ_{surf} obtained from the reflectivity measurements (open circles) and the FWHM of the rocking curves (solid circles) versus the reduced temperature T_S/T_M for Pt films 100 Å thick.

Figure 10 shows the dependencies of the surface roughness σ_{surf} as obtained from the reflectivity measurements (open circles) and the FWHM of the rocking curve (solid circles) versus the reduced temperature T_S/T_M for films 100 Å thick, where T_M is the

melting temperature for platinum (1772 °C). Two temperature ranges with changing film microstructure have been identified. At the substrate temperatures $T_S = 30$ °C and $T_S = 300$ °C the platinum films grow very smoothly. On the other hand, the values of the FWHM point to a state of disorder at the low substrate temperatures $T_S = 30$ °C and $T_S = 100$ °C, with polycrystalline properties without any texture. Only near 200 °C does the texture appear, and for higher substrate temperatures T_S nearly ideal Laue oscillations of the (111) Bragg peak have been observed. Although the in-plane mosaicity is still rather large, the in-plane Pt axes are strongly correlated with the substrate axes on a macroscopic scale. This result is supported by the growth of Pt/Al_2O_3 multilayers with high-quality structure of the Pt layers and with the same epitaxial alignment of the Pt on sapphire [19].

This behaviour seems to be universal for many metallic films when compared to the reduced temperature T_S/T_M [20]. For thick films deposited at high deposition rates ($R > 100$ Å s^{-1}), a few temperature zones have been found, each of which is characterized by a different type of microstructure [21, 22]. For $T_S < 0.3T_M$, film growth proceeds by ballistic aggregation and the internal structure is porous and contains a high density of dislocations. For $0.3T_M < T_S < 0.5T_M$, columnar grains, which extend vertically through the film, are formed. The lateral grain size increases with increasing T_S and the microstructure is mainly controlled by a large surface diffusion.

Although this classification scheme has been applied for high deposition rates, a computer simulation shows that the transition temperatures depend on the deposition rate [23]. The slower surface diffusion at lower T_S can be compensated by a longer time of migration of adatoms to build up a monolayer. From the experimentally established boundary temperature $T_1 \approx 0.3T_M$ for $R \approx 1000$ Å s^{-1}, a smaller $T_1 \approx 0.21T_M$ is obtained for $R \approx 1$ Å s^{-1} [23]. One should not place too much reliance on the good agreement with the transition to crystallinity at $T_1 \approx (0.24 \pm 0.03)T_M$ for the Pt films, but it does indicate that this model should also be applicable in our case.

For films grown at $T_S = 600$ °C ($T_S/T_M = 0.42$), island growth has been observed, and therefore we can suppose that at $T_S \sim 400$–500 °C a change in growth mode takes place. This is in accordance with the results obtained in prior work [10] in which, in the growth of platinum films by chemical vapour deposition, two growth regimes were distinguished. The activation energies suggest a reaction-controlled regime [24] ($E_{Pt} = 200$ kJ mol^{-1}) at $T_S \leqslant 470$ °C ($T_S/T_M \leqslant 0.36$) and a diffusion-controlled regime [24] ($E_{Pt} = 60$ kJ mol^{-1}) at high temperatures. However, a detailed investigation of these temperature zones should be carried out and the precise definition of the boundary temperatures should be established.

5. Conclusions

Platinum films in the thickness range 20–500 Å were sputtered onto $(11\bar{2}0)$ sapphire substrates at different substrate temperatures T_S. A correlated variation of the structural parameters with substrate temperature T_S was found. The films sputtered at $T_S = 30$ °C and 300 °C are very smooth with small values of the surface and interface roughnesses. For films grown at $T_S = 600$ °C, island growth dominates. The films deposited at $T_S \geqslant 300$ °C mainly consist of grains which were grown from the substrate up to the surface. The epitaxial relationship between the platinum film and the sapphire substrate has been determined using in-plane x-ray diffraction. It was demonstrated that Pt epitaxial films contain two in-plane orientations related by a 180° rotation. Anisotropic compression in the $[1\bar{1}0]$ direction and expansion in the [111] direction has been observed for these films. This is a result of strain in the film plane, which corresponds to a tension due to Poisson's ratio.

Acknowledgments

The authors would like to thank Professor Hartmut Zabel for fruitful discussions. The financial support for this research from the Deutsche Forschungsgemeinschaft within the Graduierten-Kolleg 'Dynamische Prozesse an Festkörperoberflächen' is gratefully acknowledged. One of us (AN) wants to thank the Ruhr-Universität Bochum for hospitality during his visit to Bochum.

References

[1] Steinrück H-P, Pesty F, Zhang L and Madey T E 1995 *Phys. Rev.* B **51** 2427
[2] Roberts S and Gorte R J 1990 *J. Chem. Phys.* **93** 5337
[3] Altman E I and Gorte R J 1988 *J. Catal.* **110** 191
[4] Farrow R F C, Harp G R, Marks R F, Rabedeau T A, Toney M F, Weller D and Rarkin S S P 1993 *J. Cryst. Growth* **133** 47
[5] Wright T R, Braeckel T R and Kizer D E 1968 *Report* AFML-TR-68-6
[6] Heiderg J, Daghighi-Ruhi R, Weyssenhoff H V and Habekost A 1988 *Mater. Res. Soc. Symp. Proc.* **101** 221
[7] Adachi M, Matsuzaki T, Yamada T, Shiosaki T and Kawabata A 1987 *Japan. J. Appl. Phys.* **26** 550
[8] Okamura T, Adachi M, Shiosaki T and Kawabata A 1991 *Japan. J. Appl. Phys.* **30** 1034
[9] Vargas R, Goto T, Zhang W and Hirai T 1994 *Appl. Phys. Lett.* **65** 1094
[10] Minvielle J, White R L, Hildner M L and Wilson R J 1996 *Surf. Sci.* **366** L755
[11] Morawe Ch, Stierle A, Metoki N, Bröhl K and Zabel H 1991 *J. Magn. Magn. Mater.* **102** 223
[12] Parratt L G 1954 *Phys. Rev.* **95** 359
[13] Névot L and Croce P 1980 *Revue Phys. Appl.* **15** 761
[14] Warren W E 1969 *X-ray Diffraction* (Reading, MA: Addison-Wesley)
[15] Stierle A, Abromeit A, Bröhl K, Metoki N and Zabel H 1992 *Surface X-Ray and Neutron Scattering* ed H Zabel and I K Robinson (Berlin: Springer) p 233
[16] Klokholm E 1969 *J. Vac. Sci. Technol.* **6** 138
[17] Sonntag P, Donner W, Metoki N and Zabel H 1994 *Phys. Rev.* B **49** 2869
[18] Doerner M F and Nix W D 1988 *CRC Crit. Rev. Solid State Mater. Sci.* **14** 225
[19] Morawe Ch and Zabel H 1995 *Appl. Phys. Lett.* **67** 2612
[20] Grovenor C R M, Hentzell H T G and Smith D A 1984 *Acta Metall.* **32** 773
[21] Movchan B A and Demchishin A V 1969 *Phys. Met. Metallogr.* **28** 83
[22] Thornton J A 1977 *Annu. Rev. Mater. Sci.* **7** 236
[23] Müller K H 1985 *J. Appl. Phys.* **58** 2573
[24] Ivanova L M and Pletyushkin A A 1967 *Izv. Akad. Nauk SSSR Neorg. Mater.* **3** 1817